ChemComm

COMMUNICATION

View Article Online
View Journal | View Issue

Cite this: *Chem. Commun.*, 2018, **54**, 10714

Received 27th May 2018,
Accepted 23rd August 2018

DOI: 10.1039/c8cc04205e

rsc.li/chemcomm

A heterobimetallic single-source precursor enabled layered oxide cathode for sodium-ion batteries†

Maofan Li,[a] Kai Yang,[a] Jiajie Liu,[a] Xiaobing Hu,[b] Defei Kong,[a] Tongchao Liu,[a] Mingjian Zhang *[ac] and Feng Pan *[a]

A single-source precursor $NaCo(acac)_3$ (acac = acetylacetone) for layered oxide cathodes of sodium-ion batteries (SIBs) is reported here. It features a 1D chain structure, and is prepared in nearly quantitative yield employing commercially available reagents. The complex is stable in open air and tends to dissolve in various strongly polar solvents, including H_2O and methanol. The phase-pure layered oxide cathode material P2-Na_xCoO_2 for SIBs is obtained through calcining the complex, and exhibits an excellent rate capability, even superior to the recently reported P2-Na_xCoO_2 microspheres. More analogue complexes could be obtained through cationic replacement for the synthesis of other high-performance layered metal oxides for SIBs.

Since the first commercialization of lithium-ion batteries (LIBs) based on $LiCoO_2$ in 1991 by Sony, LIBs have made great progress in the past 27 years and are widely used in human life such as in laptops, mobiles, electronic vehicles, *etc.*, owing to their low cost and high energy density.[1–3] As the applications of LIBs have been expanded from portable electronics to electric vehicles and grid-scale energy storages, a great concern arises about their widespread availability and rising price due to the low abundance of lithium resources on Earth. As a good alternative to LIBs, sodium-ion batteries (SIBs) with lower cost have attracted increasing attention because of the super high abundance of Na,[4–6] and its redox potential (−2.71 V *vs.* SHE) close to that of lithium (−3.03 V *vs.* SHE).[7] In fact, LIBs and SIBs were studied almost simultaneously.[8,9] In 1980, when layered $LiCoO_2$ was first reported as a cathode material for LIBs, the electrochemical activity of layered Na_xCoO_2 was also confirmed for SIBs.[10,11] From the viewpoint of the high similarity of the physical and chemical properties of lithium and sodium, Na_xCoO_2 has always been considered to be a promising cathode material for SIBs since the great success of $LiCoO_2$ for LIBs. However, the practical application of Na_xCoO_2 is hindered by its poor rate capability and cycling performance. Many efforts have been devoted to understanding and fixing this concern. *In situ* X-ray diffraction (XRD) studies demonstrated that a series of abrupt phase transformations happened during Na^+ extraction/insertion due to the great sensitivity of Na^+ ordering to the Na^+ content in the layered structure.[12,13] Several effective approaches have been developed to improve its cycling stability and rate capability, such as doping or substitution of other cations through suppressing the Na^+ ordering (*e.g.* Ca^{2+}, Ti^{4+}, Cr^{3+} and $Mn^{3+/4+}$),[14–19] and the construction of special microscopic architectures (*e.g.* microspheres).[20] All these efforts are mainly confined to the solid-state (SS) synthesis of Na_xCoO_2. Similar to the case in Li-ion batteries, the electrochemical performance of layered cathodes for Na-ion batteries is also greatly affected by the phase purity, the stoichiometry and distribution of constituent elements, the morphology uniformity and the properties of the particle surface.[21,22] Lots of efforts have been devoted to improving the electrochemical performance through elemental substitution and doping,[23–26] surface modification,[27,28] *etc.*, but little work is reported about tuning the uniformity of elemental distribution and the particle morphology partially due to the difficulty and rarity of developing new synthesis methods.

For so long, the SS method has always been the main-stream route for the synthesis of Na_xCoO_2, wherein firstly a Na source (Na_2CO_3, NaOAc, *etc.*) and a Co source (Co_3O_4, $CoCO_3$, $Co(OH)_2$, *etc.*) are mixed by grinding or ball milling, and then calcination is performed.[13,29–31] It naturally brings some concerns, such as the inhomogeneity of elemental distribution, the nonuniformity of morphologies, and the dirty surface of individual particles, which are detrimental to the final electrochemical performance of the products. Developing new synthesis routes is essential to provide opportunities to solve these issues, thereby enhancing the electrochemical performance. As an emerging method,

[a] *School of Advanced Materials, Peking University, Peking University Shenzhen Graduate School, Shenzhen 518055, China. E-mail: zhangmj@pkusz.edu.cn, panfeng@pkusz.edu.cn*
[b] *Condensed Matter Physics and Materials Science Department, Brookhaven National Laboratory, Upton, New York 11973, USA*
[c] *Sustainable Energy Technologies Department, Brookhaven National Laboratory, Upton, New York 11973, USA*

† Electronic supplementary information (ESI) available. CCDC 1864041. For ESI and crystallographic data in CIF or other electronic format see DOI: 10.1039/c8cc04205e

the single-source precursor (SP) method, combination of all the involved metal elements in one single compound with appropriate ratios, has delivered enhanced electrochemical performance in preparing cathode materials for LIBs, due to the great uniformity of elemental distribution and fancy morphologies. Layered $LiCoO_2$, spinel $LiMn_2O_4$ and layered $LiFeO_2$ have been reported by Dikarev's group.[32–34] Our group also reported multiple layered oxides for Li-ion batteries through the SP method.[35] Nevertheless, this method has never been extended to the synthesis of layered oxide cathode materials for SIBs except for the nonoxide case of $NaMF_3$ (M = Mn^{2+}, Fe^{2+}, Co^{2+} and Ni^{2+}).[36]

In this work, a carbonyl-bridged single-source precursor $NaCo(acac)_3$ (acac = acetylacetone) featuring a 1D chain structure was successfully designed and applied to achieve the layered oxide cathode material P2-Na_xCoO_2. In comparison with the conventional SS method, Na_xCoO_2 obtained *via* this SP method exhibited enhanced electrochemical performance, especially superior rate capability (70 mA h g^{-1} at the current density of 2000 mA g^{-1}), which is even superior to the recently reported spherical Na_xCoO_2 (64 mA h g^{-1} at the current density of 2000 mA g^{-1}). This could be ascribed to the great uniformity of elemental distribution at the nanometer level. This method opens a new avenue to prepare high-performance layered metal oxide cathodes for SIBs.

The heterometallic precursor $NaCo(acac)_3$ was synthesized *via* the solution reflux method (Fig. S1, ESI†). Initially the below reaction was followed:

$$3Na(acac) + CoCl_2 \rightarrow NaCo(acac)_3 + 2NaCl \quad (1)$$

This reaction affords two products $NaCo(acac)_3$ and NaCl, which are hard to dissolve in ethanol and readily dissolve in strongly polar solvents, such as H_2O and methanol. It is hard to find an appropriate solvent to achieve pure $NaCo(acac)_3$. One method to solve this issue is utilizing the sublimation character of $NaCo(acac)_3$ at temperatures below the decomposition temperature to purify it (Fig. S5, ESI†). The other method is using a commercially available reagent $Co(acac)_2$ to replace $CoCl_2$ to obtain pure $NaCo(acac)_3$ without any additional purification by following reaction (2).

$$Na(acac) + Co(acac)_2 \rightarrow NaCo(acac)_3 \quad (2)$$

As shown in Fig. S2 (ESI†), the pink powder of $NaCo(acac)_3$ can be readily collected in nearly quantitative yield within several hours at a low temperature (55 °C), making it attractive for large-scale application. As shown in Fig. 1a, the purity has been confirmed by comparing the X-ray powder diffraction (XRD) pattern with the calculated one from the single crystal data (Tables S2–S5, ESI†). The product was observed to be stable under ambient conditions and can be handled without using a glovebox for further studies.

The single crystals, presenting a prism shape with orange color (Fig. S3, ESI†), were grown using the vapor diffusion method (see the ESI†). X-ray diffraction studies revealed the crystal structure of $NaCo(acac)_3$, shown in Fig. 1c. It crystalized in the space group $R\bar{3}c$,[37] the same with its analogue $LiCo(acac)_3$.[34] As we can see, it was constructed by a lot of parallel-aligned 1D chains along the *c* axis, which consisted of alternately connected Na^+ and

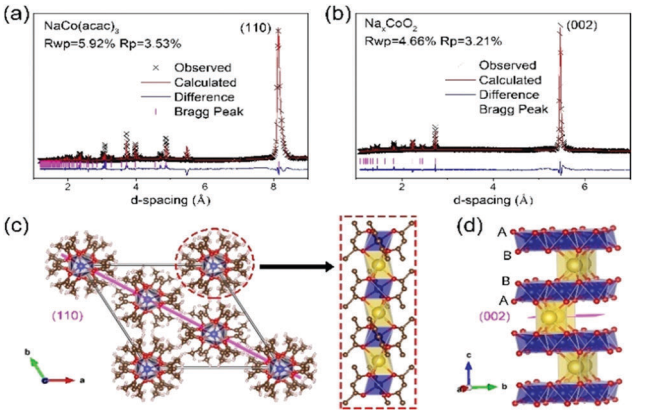

Fig. 1 Experimental and refined XRD patterns of $NaCo(acac)_3$ (a) and Na_xCoO_2 (b); the structural sketch maps of $NaCo(acac)_3$ (c) and Na_xCoO_2 (d).

[$Co(acac)_3$] units. Therein, Co^{2+} cations exhibit an octahedral geometry with six oxygens from the three chelating acac molecules, and Na^+ ions present a trigonal prism geometry with six oxygen atoms from the six acac molecules.

Na_xCoO_2 was obtained by calcining $NaCo(acac)_3$ at 850 °C in air. The powder XRD pattern is illustrated in Fig. 1b. Rietveld refinement was performed by using P2-type $NaCoO_2$ with space group $P6_3/mmc$ (ICSD 246585), respectively. The detailed refinement parameters for XRD patterns are shown in Table S5 (ESI†). As shown in Fig. 1d, P2-Na_xCoO_2 presents an AB BA oxygen packing structure with cobalt ions in the octahedral sites and Na^+ ions in the octahedral or prismatic sites. Accordingly, the NaO_6 octahedra and CoO_6 octahedra in the precursor are the basic structural units to produce the layered oxides Na_xCoO_2. The similarity of the basic structural units ensures the successful phase transformation from the precursor $NaCo(acac)_3$ to P2-Na_xCoO_2.

The morphologies of the precursor $NaCo(acac)_3$ and the product P2-Na_xCoO_2 were investigated by SEM and TEM characterization. As shown in Fig. 2a, the precursor presented a uniform prism shape, with a length of about 3–5 μm and a width of about 100–200 nm. This shape was well consistent with their hexagonal crystal structure shown in Fig. 1c, because the crystals preferred to grow along the *c* axis by extending the 1D chain. The product Na_xCoO_2 presented a uniform hexagonal thick-plate shape with a diameter of about 5–10 μm and a thickness of about 2–4 μm, as shown in Fig. 2b. Fig. 2c shows the high resolution TEM image. The indexing of the (002) crystallographic planes indicated that the thick plate was constructed by parallelly stacking lots of single thin slabs along the *c* axis, which might be beneficial for Na^+ fast de/intercalation to enhance the rate capability. As shown in Fig. 2d, the selected-area electron diffraction (SEAD) pattern revealed the existence of superlattices in Na_xCoO_2 as an intrinsic bulk characteristic. This superlattice structure indicated Na^+/vacancy ordering between CoO_2 layers, which has been reported to take place at a certain sodium content.[38–40] By comparing the TEM images in Fig. S8 (ESI†), a much cleaner surface was obtained for Na_xCoO_2 prepared *via* the SP method compared to that prepared *via* the SS method, which may be beneficial for the fast Na^+ de/intercalation during the electrochemical tests.

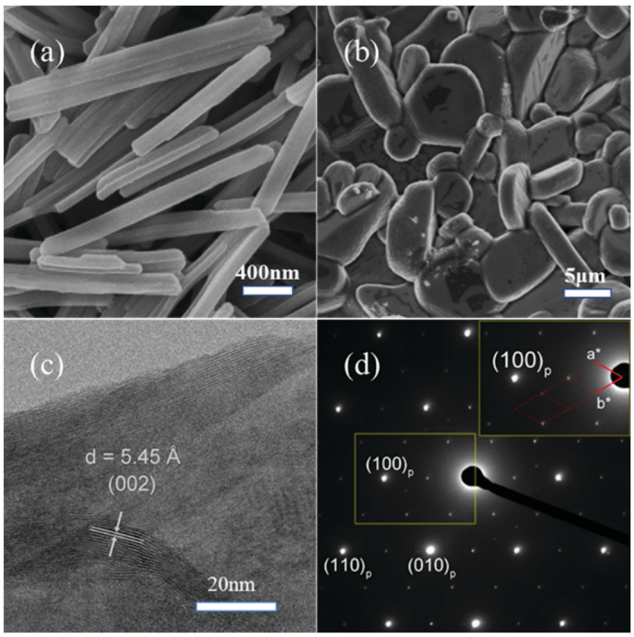

Fig. 2 SEM images of $NaCo(acac)_3$ (a) and Na_xCoO_2 (b); (c) high resolution TEM image of Na_xCoO_2; (d) selected-area electron diffraction (SAED) pattern of Na_xCoO_2.

The entire morphology evolution process from $NaCo(acac)_3$ to P2-Na_xCoO_2 was tracked using SEM images in Fig. 3a. From RT to 200 °C, the prism shape of $NaCo(acac)_3$ was basically preserved, but every individual prism decomposed into lots of nanoparticles, which was identified as spinel Co_3O_4 and some kind of unknown Na source using the XRD pattern in Fig. S6 (ESI†). The high uniformity in the mixture of the Na source and Co source at the nanometer level is demonstrated here. This kind of superiority, which usually could not be achieved by grinding or ball-milling in the traditional SS method, provides the basis for the superiority of the SP method. As the temperature was elevated to 400 °C, the prism shape completely disappeared, and nanosized particles merged and grew into sub-micrometer particles with a size of around 100–500 nm. With further increase in temperature up to 600 °C, the particle size increased to 500–1000 nm, and the phase completely transformed to P3-Na_xCoO_2. Finally, the layered P2-Na_xCoO_2 with high crystallinity and a larger particle size was obtained at 850 °C, presenting the regular hexagonal plate shape. The multi-step phase transition process involving a P3 intermediate phase was similar to the traditional SS method.[41,42] Correspondingly, the multi-step thermal decomposition process during the calcination was also observed *via* the TGA/DSC curves of $NaCo(acac)_3$ in Fig. S4 (ESI†). The elemental uniformity of $NaCo(acac)_3$ and Na_xCoO_2 was further confirmed by SEM and TEM EDX elemental mappings (Fig. S7, ESI† and Fig. 3b).

Finally, Na_xCoO_2 samples prepared *via* the SP and SS methods were both assembled into half cells to test their electrode performance. The galvanostatic charge and discharge performance was tested at various current densities (10, 20, 50, 100, 200, 500, 1000, and 2000 mA g^{-1}), as shown in Fig. 4a, for determining the rate tolerance of the materials. Five cycles were performed at each current density and finally returned to 100 mA g^{-1}. At 10, 20, 50, 100, 200, 500, 1000, 2000, and 100 mA g^{-1}, the average discharge capacities for the five cycles are 101.7, 105.3, 105.9, 104.0, 101.1, 93.6, 82.7, 69.9, and 100.8 mA h g^{-1} for Na_xCoO_2 prepared *via* the SP method, obviously higher than the corresponding values for Na_xCoO_2 prepared *via* the SS method. The cells both showed higher capacities when the current density increased from 10 to 20 and 50 mA g^{-1}, a similar phenomenon was previously reported in lithium ion battery cathode materials, and this may be related to an activation process of P2-Na_xCoO_2 during the first several cycles.[43,44] Fig. 4b depicts the charge/discharge profiles of Na_xCoO_2 at different current densities, which were extracted

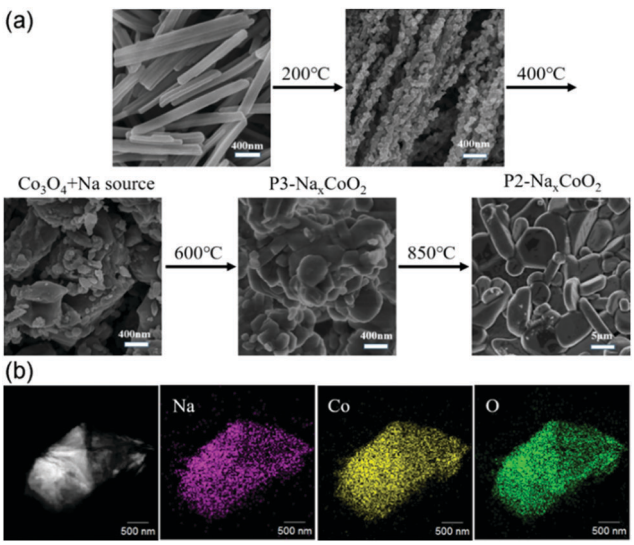

Fig. 3 (a) The SEM images for $NaCo(acac)_3$ calcined at different temperatures to show the morphology evolution from the precursor $NaCo(acac)_3$ to the product Na_xCoO_2; (b) the TEM EDX mapping for a single particle of Na_xCoO_2.

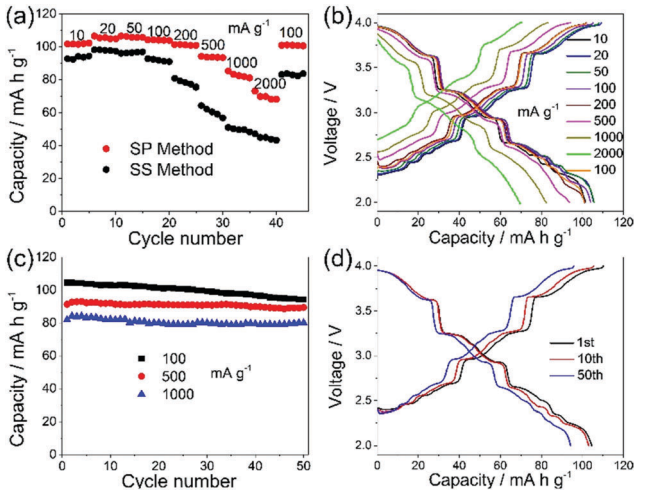

Fig. 4 Electrochemical performance of Na_xCoO_2. Rate performance of P2-Na_xCoO_2 prepared *via* the SP and SS methods (a); charge and discharge profiles with different current densities for P2-Na_xCoO_2 prepared *via* the SP method (b); cycling performance with current densities of 100, 500 and 1000 mA g^{-1} (c); and charge and discharge profiles at selected cycles with a current density of 100 mA g^{-1} for P2-Na_xCoO_2 prepared *via* the SP method (d).

from the third cycle of every five cycles. At 10 mA g^{-1}, anodic and cathodic plateaus are clearly visible at 4.00, 3.70, 3.31, 3.19, 3.00, 2.73, 2.67, 2.62, 2.55 and 3.93, 3.62, 3.20, 3.13, 2.90, 2.60, 2.55, 2.47, 2.33 V, respectively. These plateaus are quite consistent with the redox couples observed in cyclic voltammetry (CV) studies at 0.3 mV s^{-1} in Fig. S10 (ESI†). As shown in Table S7 (ESI†), the excellent rate performances reported here are better than the performances of all those Na_xCoO_2 prepared *via* the SS method in earlier reports,[29–31] and even superior to the recently reported spherical Na_xCoO_2 (64 mA h g^{-1} at the current density of 2000 mA g^{-1}).[20] The cycling stability for Na_xCoO_2 prepared *via* the SP method was tested with current densities of 100, 500 and 1000 mA g^{-1}. Fig. 4c shows very good capacity retentions, 90%, 96%, and 95% after 50 cycles, respectively. The charge/discharge profiles in Fig. 4d show a ladder-like behavior, which is also supported by earlier reports.[14–16,30] The charge/discharge capacities of 1, 10 and 50 cycles are 110.1/104.6, 105.3/103.1 and 95.8/94.2 mA h g^{-1}, respectively. According to the previous reports, the cycling stability could be further improved by doping other elements, such as Ca^{2+} and Ti^{4+}.[14,30]

In summary, a heterometallic single-source precursor $NaCo(acac)_3$ was successfully designed and prepared for the synthesis of P2-Na_xCoO_2 for SIBs. When acting as a cathode for SIBs, it exhibited excellent electrochemical performance, especially the superior rate capability, which could be ascribed to the great uniformity of particle morphology and the clean particle surface. It provides a unique and valuable approach to prepare high performance electrode materials for SIBs. More layered Na-ion cathode materials, such as P2-$Na_{0.7}MnO_2$, O3-$NaFeO_2$ and $Na_x(Ni/Co/Mn)O_2$, even including layered K-ion materials, are expected to be prepared using this method.

This work was supported by the Guangdong Innovative Team Program (2013N080), the Peacock Plan (KYPT20141016105435850), the Shenzhen Science and Technology Research Grant (JCYJ20151015162256516 and JCYJ20150729111733470), the Chinese Postdoctoral Science Foundation (2015M570882 and 2015M570894), the International Postdoctoral Exchange Fellowship Program (No. 53 Document of OCPC, 2016), and the U. S. Department of Energy (DOE) Office of Energy Efficiency and Renewable Energy under the Advanced Battery Materials Research (BMR) program (DE-SC0012704).

Conflicts of interest

There are no conflicts to declare.

Notes and references

1 M. S. Whittingham, *Chem. Rev.*, 2014, **114**, 11414–11443.
2 M. Armand and J. M. Tarascon, *Nature*, 2008, **451**, 652–657.
3 M. M. Thackeray, C. Wolverton and E. D. Isaacs, *Energy Environ. Sci.*, 2012, **5**, 7854–7863.
4 V. Palomares, P. Serras, I. Villaluenga, K. B. Hueso, J. Carretero-Gonzalez and T. Rojo, *Energy Environ. Sci.*, 2012, **5**, 5884–5901.
5 S. W. Kim, D. H. Seo, X. H. Ma, G. Ceder and K. Kang, *Adv. Energy Mater.*, 2012, **2**, 710–721.
6 N. Yabuuchi, K. Kubota, M. Dahbi and S. Komaba, *Chem. Rev.*, 2014, **114**, 11636–11682.
7 S. P. Ong, V. L. Chevrier, G. Hautier, A. Jain, C. Moore, S. Kim, X. H. Ma and G. Ceder, *Energy Environ. Sci.*, 2011, **4**, 3680–3688.
8 M. S. Whittingham, *Prog. Solid State Chem.*, 1978, **12**, 41–99.
9 G. H. Newman and L. P. Klemann, *J. Electrochem. Soc.*, 1980, **127**, 2097–2099.
10 K. Mizushima, P. C. Jones, P. J. Wiseman and J. B. Goodenough, *Mater. Res. Bull.*, 1980, **15**, 783–789.
11 C. Delmas, J. J. Braconnier, C. Fouassier and P. Hagenmuller, *Solid State Ionics*, 1981, **3–4**, 165–169.
12 M. Roger, D. J. P. Morris, D. A. Tennant, M. J. Gutmann, J. P. Goff, J. U. Hoffmann, R. Feyerherm, E. Dudzik, D. Prabhakaran, A. T. Boothroyd, N. Shannon, B. Lake and P. P. Deen, *Nature*, 2007, **445**, 631–634.
13 R. Berthelot, D. Carlier and C. Delmas, *Nat. Mater.*, 2011, **10**, 74–80.
14 S. M. Kang, J. H. Park, A. Jin, Y. H. Jung, J. Mun and Y. E. Sung, *ACS Appl. Mater. Interfaces*, 2018, **10**, 3562–3570.
15 Y. S. Wang, R. J. Xiao, Y. S. Hu, M. Avdeev and L. Q. Chen, *Nat. Commun.*, 2015, **6**, 6945.
16 N. Sabi, A. Sarapulova, S. Indris, H. Ehrenberg, J. Alami and I. Saadoune, *ACS Appl. Mater. Interfaces*, 2017, **9**, 37778–37785.
17 G. F. Gao, D. Tie, H. Ma, H. J. Yu, S. S. Shi, B. Wang, S. M. Xu, L. L. Wang and Y. F. Zhao, *J. Mater. Chem. A*, 2018, **6**, 6675–6684.
18 J. Y. Hwang, S. T. Myung, J. U. Choi, C. S. Yoon, H. Yashiro and Y. K. Sun, *J. Mater. Chem. A*, 2017, **5**, 23671–23680.
19 H. Park, J. Kwon, H. Choi, T. Song and U. Paik, *Sci. Adv.*, 2017, **3**, e1700509.
20 Y. J. Fang, X. Y. Yu and X. W. Lou, *Angew. Chem., Int. Ed.*, 2017, **56**, 5801–5805.
21 P. F. Wang, Y. You, Y. X. Yin and Y. G. Guo, *Adv. Energy Mater.*, 2018, **8**, 1701912.
22 Y. You and A. Manthiram, *Adv. Energy Mater.*, 2018, **8**, 1701785.
23 D. Buchholz, C. Vaalma, L. G. Chagas and S. Passerini, *J. Power Sources*, 2015, **282**, 581–585.
24 Z. Y. Li, H. B. Wang, D. F. Chen, K. Sun, W. Y. Yang, J. B. Yang, X. F. Liu and S. B. Han, *ChemSusChem*, 2018, **11**, 1223–1231.
25 C. Zhang, R. Gao, L. R. Zheng, Y. M. Hao and X. F. Liu, *ACS Appl. Mater. Interfaces*, 2018, **10**, 10819–10827.
26 Y. You, S. O. Kim and A. Manthiram, *Adv. Energy Mater.*, 2017, **7**, 1601698.
27 J. Zhang and D. Y. W. Yu, *J. Power Sources*, 2018, **391**, 106–112.
28 L. Q. Mu, M. M. Rahman, Y. Zhang, X. Feng, X. W. Du, D. Nordlund and F. Lin, *J. Mater. Chem. A*, 2018, **6**, 2758–2766.
29 J. J. Ding, Y. N. Zhou, Q. Sun, X. Q. Yu, X. Q. Yang and Z. W. Fu, *Electrochim. Acta*, 2013, **87**, 388–393.
30 S. C. Han, H. Lim, J. Jeong, D. Ahn, W. B. Park, K. S. Sohn and M. Pyo, *J. Power Sources*, 2015, **277**, 9–16.
31 B. V. R. Reddy, R. Ravikumar, C. Nithya and S. Gopukumar, *J. Mater. Chem. A*, 2015, **3**, 18059–18063.
32 A. Navulla, L. Huynh, Z. Wei, A. S. Filatov and E. V. Dikarev, *J. Am. Chem. Soc.*, 2012, **134**, 5762–5765.
33 H. X. Han, Z. Wei, M. C. Barry, A. S. Filatov and E. V. Dikarev, *Dalton Trans.*, 2017, **46**, 5644–5649.
34 Z. Wei, H. X. Han, A. S. Filatov and E. V. Dikarev, *Chem. Sci.*, 2014, **5**, 813–818.
35 M. F. Li, J. J. Liu, T. C. Liu, M. J. Zhang and F. Pan, *Chem. Commun.*, 2018, **54**, 1331–1334.
36 Z. Wei, A. S. Filatov and E. V. Dikarev, *J. Am. Chem. Soc.*, 2013, **135**, 12216–12219.
37 X. B. Li, G. Musie and D. R. Powell, *Acta Crystallogr., Sect. E: Struct. Rep. Online*, 2003, **59**, M717–M718.
38 H. X. Yang, C. J. Nie, Y. G. Shi, H. C. Yu, S. Ding, Y. L. Liu, D. Wu, N. L. Wang and J. Q. Li, *Solid State Commun.*, 2005, **134**, 403–408.
39 S. Hwang, Y. Lee, E. Jo, K. Y. Chung, W. Choi, S. M. Kim and W. Chang, *ACS Appl. Mater. Interfaces*, 2017, **9**, 18883–18888.
40 F. T. Huang, M. W. Chu, G. J. Shu, H. S. Sheu, C. H. Chen, L. K. Liu, P. A. Lee and F. C. Chou, *Phys. Rev. B: Condens. Matter Mater. Phys.*, 2009, **79**, 014413.
41 M. Blangero, D. Carlier, M. Pollet, J. Darriet, C. Delmas and J. P. Doumerc, *Phys. Rev. B: Condens. Matter Mater. Phys.*, 2008, **77**, 184116.
42 L. W. Shacklette, T. R. Jow and L. Townsend, *J. Electrochem. Soc.*, 1988, **135**, 2669–2674.
43 M. G. Lazarraga, L. Pascual, H. Gadjov, D. Kovacheva, K. Petrov, J. M. Amarilla, R. M. Rojas, M. A. Martin-Luengo and J. M. Rojo, *J. Mater. Chem.*, 2004, **14**, 1640–1647.
44 L. Zhou, D. Y. Zhao and X. W. Lou, *Angew. Chem., Int. Ed.*, 2012, **51**, 239–241.